

Pressure and temperature effects over the electrical and magnetic properties of FeSi: a DFT+DMFT study

Paromita Dutta^{1,*} and Sudhir K. Pandey^{2,†}

¹*School of Basic Sciences, Indian Institute of Technology Mandi, Kamand, Himachal Pradesh-175005, India*

²*School of Engineering, Indian Institute of Technology Mandi, Kamand, Himachal Pradesh-175005, India*

(Dated: July 25, 2019)

Many studies have been performed for understanding the underlying rich physics for various anomalous physical properties of FeSi. The origin of the properties are of great interest due to their still elusive theoretical understandings. Moving into this direction, we are studying the effects of pressure and temperature on the electrical and magnetic properties of FeSi. For the study, electronic structure calculations of FeSi are carried out by using DFT+DMFT method with spin-orbit coupling inclusion. The self-consistently calculated values of U and J are used. Using the free energy obtained from DMFT technique at 300 K, the calculated values of lattice parameter (a_0) and bulk modulus (B_0) are ~ 4.32 Å and 110 GPa, respectively, and they are found to lie in the range of experimental values. At DFT level, the bandgap of the material is found to be increasing with pressure increment say ~ 59 meV to 102 meV corresponding to unit cell volumes of ~ 612 to 507 Bohr³, respectively. However at DMFT level, the bandgap is filled with incoherent states at 300 K, but with the application of pressure decrement of charge carriers (n) around the Fermi level is observed. Thus, predicting metal-insulator transition (MIT) to occur at ~ 300 K with increase in pressure. From momentum resolved spectral functions, the excitations are found to be more coherent with increasing pressure. This study reveals the unusual behavior of the magnetic susceptibility around 100-300 K region. The decrement behavior in spin susceptibility (χ) is found to be similar to n decrement with rise in pressure, and appears to follow $\frac{\chi^3}{n} = \text{constant}$ relation for ~ 100 K; suggesting FeSi to be Pauli paramagnetic at ~ 100 K while not the case around 300 K and above.

I. INTRODUCTION

The physical properties of numerous materials are easily explained by modern solid-state physics, such as simple metals and some conventional semiconductors and insulators^{1,2}. But, there are materials with d and f electrons, which occupy narrow orbitals have shown properties that are difficult to be explained¹. The d and f electrons experience strong Coulombic repulsion due to their spatial confinement in d and f orbitals, respectively. Such strongly interacting or correlated electrons are mostly found in transition metals and their oxides. This family of materials is called as strongly correlated electron system where profound effect of correlations on materials' properties are observed¹. The complex interplay of electron-electron interactions, kinetic energy and the d and f electrons' internal degrees of freedom i.e., spin, charge and orbital moment are incredibly rich that make the materials to exhibit complex and exotic properties¹⁻³. As a result of this interplay, various phase transitions takes place within the material which are extremely sensitive to small changes in external parameters such as temperature, pressure, electronic composition, electric field or magnetic field. It seems that if one tries to use this sensitivity towards external parameters, then it might be possible to explore the materials of this family.

The new phases have also shown surprising and useful properties such as high temperature superconductivity, heavy Fermion behavior, giant magneto-resistance, large thermoelectric response, dramatic effects in resis-

tivity across metal-insulator transitions and so on. For instance, when FeSi is electron doped by the substitution of Fe with Co, a metal-insulator transition is occurred at around $x \sim 0.02$ in $\text{Fe}_{1-x}\text{Co}_x\text{Si}$ ^{4,5} while in the wide doping range $0.05 \leq x \leq 0.07$, a helical magnetic phase emerges at low temperatures similar to MnSi ^{5,6}. A positive magneto-resistance and a large anomalous Hall effect in $\text{Fe}_{1-x}\text{Co}_x\text{Si}$ have been reported^{7,8}. Band structure calculations have shown the gap and a transition to metallic phase is observed in $\text{FeSi}_{1-x}\text{Ge}_x$ at critical concentration $x_c \sim 0.25$ ⁹⁻¹¹. It is also concluded that on application of external pressure over FeGe might induce an isostructural transition from a metallic to an insulating state¹². Further, it is reported for FeGe that volume compression suppresses the long-range magnetic order, showing strong deviations from the Landau-Fermi liquid (LFL)¹². All the above examples and our earlier works¹³⁻¹⁶ indicate that the mentioned controllable parameters can be used as probe to understand the unusual phenomena and the underlying physics behind their various exotic properties.

FeSi belongs to the family of transition metal silicides which crystallizes into noncentrosymmetric cubic B20 structure. This family possesses variety of complex phenomena which have applications in the field of applied sciences^{7,17,18}. FeSi has been under study for decades due to its temperature dependent magnetic and electrical properties^{2,19-30}. Since its discovery, FeSi has been a controversial material due to its unusual physical properties. It has an insulating ground state, and its electrical conductivity measurement shows the semi-

conductor to metal transition at ~ 200 K^{5,26–29,31}. One of its peculiar property is its magnetic susceptibility ($\chi(T)$) which is increasing with temperature rise after 100 K and has a broad maximum around ~ 500 K and then it drops; follows Curie-Weiss law at higher temperature²⁰. However, absence of spin ordering at lower temperatures is observed as its $\chi(T)$ vanishes below 50 K²². Moreover, its $\chi(T)$ value decreases rapidly as the temperature is lowered below 500 K and thought it to be the onset of anti-ferromagnetic behavior below this temperature²⁰. However, neutron scattering, Mössbauer, and NMR measurements showed no long-range magnetic order^{21,22}. A similar anomalous behavior is observed for specific heat ($c(T)$)²⁰. The electronic component of $c(T)$ has shown a broad peak at ~ 200 K, which is around the temperature where the steep increment of $\chi(T)$ with temperature rise is observed. Considering the ambiguities associated with high-temperature works (both past and present), many theoretical (modelistic) and experimental studies have been done over this FeSi system^{20,23–25,32–35}. The first attempt for the explanation of $\chi(T)$ and $c(T)$ was given by Jaccarino *et al.*²⁰. Their theory consisted of two models out of which second one seemed to be probably correct, and the second model considered the local excitations between Fe singlet (S=0) and spin doublet (S=1/2) or spin-triplet (S=1) states. Then, another explanation for $\chi(T)$ was given by Takahashi *et al.*²⁴, they proposed a temperature-induced local-moment model based on their spin-fluctuation theory. Based on this theory FeSi was described as a nearly ferromagnetic semiconductor^{23–25}. This model was then supported from the neutron-scattering measurements as performed by Shirane *et al.* group³³. However, Oh *et al.* group, could not find the indication of temperature-induced localized moments at high temperatures in the Fe 3s core-level spectra³⁴.

Yet, another attempt was called upon Kondo-insulator model^{31,36–39} for the explanation of $\chi(T)$. This attempt was made due to the similarity found between the spin-fluctuation spectra of CeNiSn and FeSi³⁷. According to this model, atomic-like localized electron levels interact with wide itinerant bands where their hybridization is quite weak. But according to Mattheiss *et al.* work³⁵, the hybridization between Fe 3d and Si 3s or 3p was found to be very strong; making this model as applied on FeSi to be more questionable. Further another approach was given by Varma⁴⁰, where he considered the concept of intermediate valence. In this approach, the ground state was claimed to be $d^6\text{Fe}^{2+}$ hybridized with Si leading to spin zero and $d^7\text{Fe}^{1+}$ to be the lowest excited state with spin 3/2. This gives the explanation of high temperature magnetic behavior with the theory of thermally induced intermediate valence of Fe in FeSi. Thus, we can see that there are so many controversies associated with the explanations for the anomalous behavior of temperature dependent magnetic response of FeSi. Out of these studies, many were mainly concentrated on interpreting the $\chi(T)$ behavior below 500 K but still

its an elusive topic that needed to be understood thoroughly which may be accomplished if studied with tunable parameters such as carrier-concentration, pressure etc. Recently, moving in this direction, strong electron-electron correlations in FeSi have been invoked by using DFT+Dynamical mean field theory (DMFT) technique where temperature is taken as a key to understand the unusual properties^{41–45}. These studies shown that the electronic correlations play an important role in elucidating the confusion that whether FeSi belongs to Kondo family or not. Likewise, DFT+DMFT results have shown the importance of electronic correlation effects in understanding the semiconductor with narrow bandgap than the concept of Kondo-insulator^{44,46}. However, the origin and the reason behind the $\chi(T)$ behavior around 100-300 K and above for the system is still unexplored. To target this aspect mainly, here we have chosen external pressure. As we know pressure decreases the inter-atomic distances making the transfer/hopping interaction (t) term to increase. It is also known that hopping interaction (t) and the Coulomb repulsion (U) are the two fundamental parameters that characterize the electronic structures of strongly correlated electron systems². Strongly correlated systems exhibit complex physical properties due to the presence of competing interaction terms in their Hamiltonian. Basic competition is lying between the tendency towards localization (leading to atomic-like behavior) and delocalization (leading to band formation). This family of materials has various physical properties which are sensitive to several external parameters, and leading to changes such as phase separations and formation of complex patterns². Now, DFT based on simple band theory (where t is taken into primarily while electronic correlations are taken on average) is used for carrying out the electronic structure calculations of FeSi. It was found to have semi-conducting gap as ground state^{20,22,35,47–58}. On other side, when U was taken into consideration explicitly with temperature effect, the band-gap found to be filled with incoherent states and predicted to be metallic theoretically and experimentally^{41,43–45,59}. Generally, in solids this U parameter becomes effective Coulomb interaction (U_{eff}) which contains the informations regarding screening coming from other orbitals. This U_{eff} has dependence on the overlapping of the orbitals. Thus, it will be interesting to see the effect of pressure by modifying the lattice parameter plus with the inclusion of temperature effect for exploring the magnetic property of FeSi. Here, it appears that taking pressure and temperature simultaneously might help in understanding the elusive $\chi(T)$ behavior and to explore the material more extensively.

In this report, we have shown the effect of pressure over FeSi system at three distinct temperatures (T=100, 300 & 800 K) with inclusion of spin-orbit coupling + electronic correlations by using DFT+DMFT technique⁶⁰. Here, we have aimed to resolve the $\chi(T)$ behavior around 100-300 K mainly by taking pressure and temperature both as important tool simultaneously. At the same time,

we have also calculated the a_0 and B_0 values ($\sim 4.32 \text{ \AA}$ and 110 GPa), which are fairly in good agreement with the experimental values as calculated by using free energy as evaluated from DMFT technique^{60,61} at 300 K. Normally, pressure tends to increase the bandwidths resulting in closing the gap between the bands. But here, from DFT calculations, we have found the bandgap to increase with increment in pressure from the volumes ~ 612 to 507 Bohr^3 with gaps ~ 59 to 102 meV , respectively. On other hand, from DMFT calculations, at 300 K the bandgap got filled with incoherent states but with pressure application there is decrement in charge carriers around the Fermi level is observed. Further, predicting MIT to occur at $\sim 300 \text{ K}$ with increase in pressure. The lifetime of the quasi-particles increases with pressure increase, indicating the existence of more coherent states. Next, we have studied the charge carrier concentration (responsible for conduction mainly) and seems to give appropriate result as given by the experimental Hall coefficient measurement³². With the study of spin susceptibility, we have revealed the unusual behavior of magnetic susceptibility of FeSi around 100-300 K; predicting the material to be Pauli-paramagnetic around 100 K.

II. COMPUTATIONAL DETAILS

The electronic structure calculations with the inclusion of spin-orbit coupling (SOC) for FeSi have been carried out. Three different calculations are performed *viz.* (i) volume-optimization of the structure by using DFT, (ii) spin-polarized calculation of onsite Coulomb interaction (U_{eff}) for different unit cell volumes by using constrained DFT method^{62,63} and (iii) structure calculations by using DFT and DFT+DMFT techniques. DFT part of the calculations is performed by the usage of full-potential linearized augmented plane-wave (FP-LAPW) method accomplished by WIEN2k code⁶⁴. DFT+DMFT calculations are performed by the WIEN2k code and the code as implemented by Haule *et al.*⁶⁰. Here, DFT+DMFT functional is implemented in the real space embedded DMFT approach⁶⁰, which delivers stationary free energies at finite temperatures⁶¹. The initial lattice constants are taken from the literature⁶⁵. For the exchange-correlation functional local density approximation (LDA) is chosen here⁶⁶. The muffin-tin sphere radii of 2.18 Bohr and 1.84 Bohr for Fe and Si sites, respectively, are used. 1000 k -points mesh grid size in whole Brillouin zone has been used.

For the first part of calculations, the calculated lattice constants as provided in Table I, are computed by fitting total energy versus unit cell volume data with the Birch-Murnaghan (BM) equation of state (eos)⁶⁷. Third-order BM isothermal eos is given in the Eq.1:

$$E(V) = E_0 + \frac{9V_0B_0}{16} \left[\left\{ \left(\frac{V_0}{V} \right)^{2/3} - 1 \right\}^3 B'_0 + \left\{ \left(\frac{V_0}{V} \right)^{2/3} - 1 \right\}^2 \left\{ 6 - 4 \left(\frac{V_0}{V} \right)^{2/3} \right\} \right] \quad (1)$$

where, where E is energy, V is volume, B_0 is equilibrium bulk modulus, V_0 is volume of unit cell corresponding to minimum energy and B'_0 is pressure derivative of bulk modulus at equilibrium value. The process of volume optimization is carried out by varying lattice constants.

U_{eff} calculation of Fe $3d$ atom in FeSi for different unit cell volumes, constrained DFT method as proposed by Anisimov and Gunnarsson⁶² has been used. The proposed method is then implemented by Madsen *et al.*⁶³. We have followed the same procedure for evaluating U_{eff} for different cell volumes as given in our earlier works⁶⁸⁻⁷¹. Here, it is important to note that the evaluated values of U_{eff} for different cell volumes are almost same as previously⁶⁸ calculated for the unit cell volume of 612 Bohr^3 . A difference of $\sim 0.2 \text{ eV}$ is found, and thus, the self-consistently calculated values of U_{eff} and J with 4.4 eV and 0.89 eV, respectively, are used⁶⁸.

DFT+DMFT calculations are carried out due to its treatment while describing the itinerant and localized behavior of the correlated electrons on equal footing. DMFT calculations are performed for 100 K, 300 K and 800 K temperatures, and these calculations are fully self-consistent in electronic charge density and impurity levels. For solving the auxiliary impurity problem, a continuous-time quantum Monte Carlo impurity solver has been used⁷². The scheme for exact double-counting as proposed by Haule has been used here⁷³. Fe $3d$ orbitals are treated at DMFT level. For all calculations, the density-density form of the Coulomb repulsion has been used by using material specific values of U_{eff} and J . Charge/cell convergence is set below 10^{-4} electronic charge for every calculation. All these DMFT calculations are converged on the imaginary axis. Then, for obtaining the self-energy on the real axis, an analytical continuation is needed to be done. This analytical continuation is achieved by using maximum entropy method⁷⁴ for the spectra on the real axis. 2000 k -points grid is used for the density of states (DOS) calculations on both DFT and DMFT levels.

III. RESULTS AND DISCUSSION

At first, we have started with carrying out volume optimization calculations for FeSi structure by using DFT method. The obtained values for total energy difference of volume dependent energies and equilibrium volume energy ($E-E_0$) are plotted as a function of volume in Fig. 1. In the same figure, we have also shown the same energy versus volume plot for the total energy

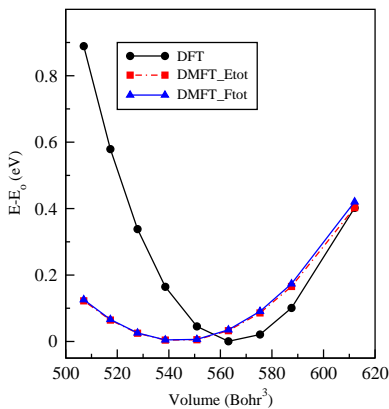


FIG. 1. (color online) Energy versus volume curve for FeSi with spin-orbit coupling for three energies as obtained from DFT, DFT+DMFT and free energy as estimated from DFT+DMFT calculations.

(DMFT_Etot) and free energy (DMFT_Ftot) as evaluated from DFT+DMFT calculations for 300 K temperature. Here, DMFT_Etot is the ground state energy calculated at absolute zero kelvin temperature while DMFT_Ftot is the free energy calculated with temperature inclusion. The calculated data are then fitted by using Birch-Murganhan (BM) equation of state⁶⁷. For the calculations, we started with the lattice constants as given in the literature⁶⁵ for the initial crystal structure. The calculated values of lattice constant (a_0) and Bulk modulus (B_0) corresponding to energies evaluated from different methods are tabulated in Table I. From the table, we can see that DFT and DMFT methods are giving almost similar a_0 values of ~ 4.37 Å and ~ 4.32 Å, respectively. When one follows the experimental a_0 values at 300 K, they are found to vary in the range of ~ 4.46 to 4.48 Å^{65,75-77}, showing ambiguity in a_0 estimation. We found that our calculated a_0 value is underestimated by ~ 0.11 Å from the experimental results. Now, when we look for the B_0 values from the Table I, it is observed that DFT happens to provide its maximum value of ~ 260 GPa whereas DMFT_Etot gives ~ 106 GPa and DMFT_Ftot of ~ 110 GPa. Experimentally B_0 values range from ~ 115 - 209 GPa at 300 K⁷⁵⁻⁷⁹. Based on this, it seems like DMFT happens to provide quite appropriate value for B_0 . Next, in Table II, we have tabulated the calculated values of pressure as computed from BM equation of state⁶⁷ for some of the volumes for which the study has been presented in the following discussion. From the Table, as one can see the difference in the calculated values of pressure corresponding to different methods for a particular unit cell volume. In-consequence of which, we are going to present the study with respect to volume only⁷⁵⁻⁷⁹. However, pressures corresponding to DMFT_Ftot can be helpful to the experimentalist if tries to perform any pressure induced experiment due to the fair closeness of B_0 with its experimental results.

TABLE I. Calculated lattice constants and Bulk modulus of FeSi for different evaluated energies.

Method	lattice constant (a_0) (Å)	Bulk modulus (B_0) (GPa)
DFT E_{tot}	4.3736	260.39
DMFT E_{tot}	4.3188	106.12
DMFT F_{tot}	4.3174	110.86

TABLE II. Calculated pressures by using BM equation state⁶⁷ of FeSi for the reduced unit cell volumes from its experimental volume = 612 Bohr³.

Unit cell volume (Bohr ³)	lattice constant (Å)	Pressure		
		DFT (GPa)	DMFT E_{tot} (GPa)	DMFT F_{tot} (GPa)
507	4.219	36.46	7.21	7.60
517	4.247	28.40	5.22	5.45
528	4.276	20.99	3.16	3.25
539	4.306	14.16	1.02	1.05
551	4.338	7.20	1.32	1.46
563	4.369	1.02	-3.67	-3.89
575	4.400	-4.47	-5.97	-6.24
588	4.432	-9.37	-8.19	-8.51
612	4.492	-17.00	-12.41	-12.78

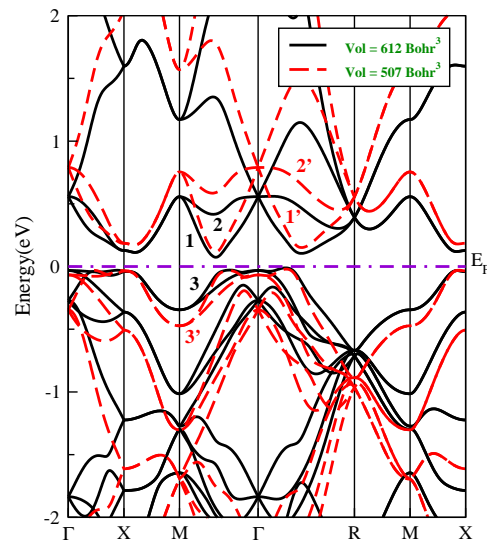


FIG. 2. (color online) Band structures of FeSi for the two volumes (a) Vol = 612 Bohr³ (solid line) and (b) Vol = 507 Bohr³ (dashed line) for the energy range ~ -2.0 eV to 2.0 eV, calculated within DFT+SOC. Zero energy corresponds to the Fermi level.

Next, we would like to understand the effect of reduced unit cell volumes over the band-structure of FeSi. For the representation, we have presented the band structures for the two extreme volumes *viz.* (i) Vol = 612 Bohr³ and (ii) Vol = 507 Bohr³ for the energy range -2.0 to 2.0 eV, calculated within DFT in Fig. 2. 612 Bohr³ is the volume of experimentally realized structure of FeSi⁶⁵. The latter one is the volume of the experimental structure when reduced by $\sim 17.17\%$. Here, one should note that the energy window is chosen on the basis of obtaining all the informations from the plot. In this plot, three bands (solid line) corresponding to Vol = 612 Bohr³ are specifically identified for the study where two of them (bands 1 & 2) lie in the conduction band (CB) region and other one (band 3) in the valence band (VB) region. Similarly, another three bands (dashed line) corresponding to Vol = 507 Bohr³ are identified as 1' & 2' (CB) and 3' (VB). From the figure, it is noticed that for the 612 Bohr³ volume, bands 1 and 2 are degenerate in the X-M direction while in the M- Γ direction they are non-degenerate. At M point bands 1 and 2 are positioned at ~ 0.55 eV while band 3 is positioned at ~ -0.34 eV. Thus, at M point the energy gap between band 1 and 3 is ~ 90 meV. The band-gap is found to be ~ 70 meV while in our previous works^{45,68} we have shown band-gap of around ~ 90 meV without SOC within DFT. This shows that inclusion of SOC has reduced the band-gap of the experimental volume. Moreover, the obtained value ~ 70 meV is quite closer to the experimental values (~ 50 meV to ~ 100 meV)^{20,47-52}. Now, when one moves from 612 to 507 Bohr³, few significant changes are observed with volume compression *viz.* (i) shifts in the energy positions of bands (ii) increased bandwidths and (iii) increment in the band-gap. These changes can be understood as when we compress the structure the lattice parameter has reduced which is making the crystal sites to come closer. In consequence of which the strength of the periodic potential has increased which has further increased the band-gap of the bands. Due to the increase in the energy gaps between the bands make them to have shifts in their energy positions. For instance, at M point the energy gap between bands 1' and 3' has increased to ~ 1.2 eV whereas earlier the gap between bands 1 and 3 is found to be ~ 0.9 eV. This has led to the shifts in the energy positions of bands 1' and 3' from bands 1 and 3 by ~ 0.2 eV and ~ 0.1 eV, respectively. Then, if we look at R point the gap between the bands 1' and 3' has increased to ~ 1.4 eV than ~ 1.0 eV. Now, the energy positions of bands 1' and 3' at R point has shifted to ~ 0.5 eV and ~ 0.9 eV. Similarly, at Γ point the energy positions of bands 1' and 2' has shifted to ~ 0.7 eV from ~ 0.5 eV. This shows that at each k -point these energy shift/gaps will be different depending upon the periodic potential strength (U_k)⁸⁰. Further, the increment in the bandwidths of the bands has been observed. This suggests the increment in the overlapping of orbitals in consequence of reduction in lattice parameter. For instance, in X-M direction the bandwidths of bands 1' and 2' has increased by ~ 0.1

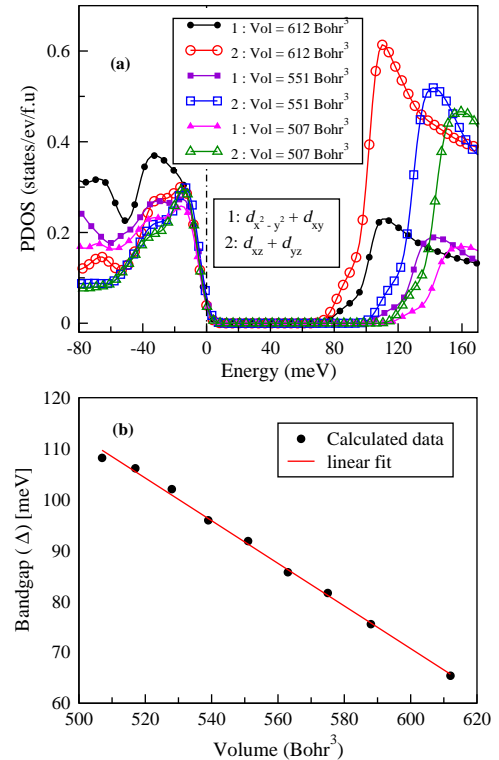


FIG. 3. (color online) (a) Partial density of states (PDOS) of the orbitals $d_{x^2-y^2} + d_{xy}$ and $d_{xz} + d_{yz}$ of Fe-3d states calculated within DFT for three different unit cell volumes 612, 551 and 507 Bohr³; zero energy corresponds to the Fermi level (dotted line), and (b) Band gap versus different unit cell volumes for the range 612-507 Bohr³ of FeSi.

eV whereas in M- Γ direction they have increased by ~ 0.1 and ~ 0.05 eV, respectively. These energy shifts/gaps and increment in their bandwidths are not uniform which further confirms that depending upon U_k these changes will vary.

For further visualization of the effect of hybridization over the band-gap, we have shown a plot of partial density of states of the orbitals $d_{x^2-y^2} + d_{xy}$ and $d_{xz} + d_{yz}$ of Fe-3d states calculated within DFT for three different unit cell volumes = 612, 551 and 507 Bohr³ in Fig. 3(a). From the plot, it is observed that with volume decrement due to large overlapping of the orbitals, the orbitals $d_{x^2-y^2} + d_{xy}$ and $d_{xz} + d_{yz}$ are moving away from the Fermi level (E_F). Likewise, the gap corresponding to both the orbitals for the experimental volume (612 Bohr³) is ~ 59 meV, then for Vol = 551 Bohr³ the gap increased to ~ 87.7 meV whereas for Vol = 507 Bohr³, it has increased to ~ 102 meV. After this, we have calculated the band-gaps corresponding to unit cell volumes ranging from 612 to 507 Bohr³ and plotted them in Fig.3(b). Then, a linear fit of the calculated data corresponding to band-gaps has been done. From the linear fit the rate of decrement of the band-gap is of ~ 0.42 meV/Bohr³; showing the decreasing trend of the

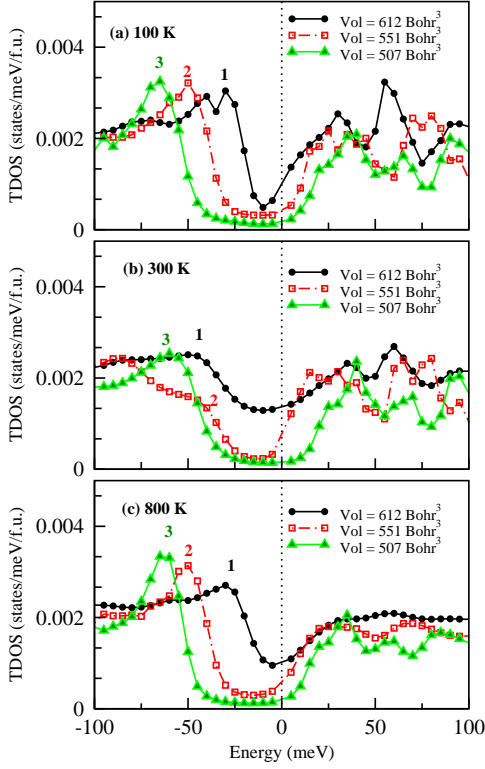


FIG. 4. (color online) Total density of states (TDOS) of FeSi calculated within DFT+DMFT for three different unit cell volumes 612, 551 and 507 Bohr³ for three different temperatures *viz.* (a) 100 K, (b) 300 K and (c) 800 K. Zero energy corresponds to the Fermi level (dotted line).

band-gaps with volume increment according to the reason stated above. Further, by extrapolating this data we have also calculated a specific unit cell volume of ~ 769 Bohr³ which corresponds to zero band-gap.

Now, in this part of discussion, we have tried to show the changes occurred in the total density of states (TDOS) of FeSi as calculated within DFT+DMFT with reduction in unit cell volumes (or increase in pressure) and temperature simultaneously. For this purpose, Fig. 4 has been drawn showing the calculated TDOS of FeSi for three different unit cell volumes 612, 551 and 507 Bohr³ for three different temperatures *viz.* (a) 100 K, (b) 300 K and (c) 800 K, respectively. For the reference, we have marked few peaks as 1, 2, and 3 lying in VB, where they correspond to Vol = 612, 551 and 507 Bohr³, respectively. Starting from 100-300 K in the Fig. 4(a) to 4(b) for the vol = 612 Bohr³, few changes are found with increase in temperature *viz.* (i) Shallowing of the deep well like feature of DOS around the E_F with increment in the finite DOS around the E_F (ii) change in the energy positions of peak 1 which has moved away from the E_F , and (iii) reduced particle-hole asymmetry. As finite DOS around the E_F is observed suggesting the material to be metallic which is different from the experimentally observed insulating behavior below 200 K²⁶⁻²⁹. There-

fore, to understand the influence of these changes over the transport behavior of the material we start with the experimental electrical resistivity (ρ) data²⁶⁻²⁹. The experimental data have shown a sharp decrement of ρ from ~ 2.5 K to 200 K suggesting it to be semi-conducting, then a slow decrement from 200-300 K and considered as a signature of weak metallic state of the material^{2,26,30}. This unusual behavior can be understood by the conductivity (σ) expression given in Eq. (2) and its relative change with respect to (w.r.t) temperature expression ($\Delta\sigma$) given in Eq. (3).

$$\sigma = \frac{ne^2\tau}{m} \quad (2)$$

$$\frac{\Delta\sigma}{\sigma} = \frac{\Delta n}{n} + \frac{\Delta\tau}{\tau} \quad (3)$$

where, e is electronic charge, m is mass of the charge carrier, n is the charge carrier concentration, τ is relaxation time, Δn and $\Delta\tau$ are the changes in the charge carrier concentration and relaxation time, respectively, w.r.t temperature. As states in the range of $k_B T$ around the E_F mostly participate in the transport of charge carriers. Thus, in Eq. (2), n will always increase while τ will always decrease with rise in temperature. Therefore, $\Delta\tau$ will always be negative with temperature increase while Δn is expected to be positive with temperature rise. When $|\frac{\Delta n}{n}| > |\frac{\Delta\tau}{\tau}|$ with temperature rise, the $\frac{\Delta\sigma}{\sigma}$ will increase and then the material will behave as semiconductor. On other hand, when $|\frac{\Delta n}{n}| < |\frac{\Delta\tau}{\tau}|$ with temperature rise, the $\frac{\Delta\sigma}{\sigma}$ will eventually decrease thereby making the material to behave as metal. However, if $|\frac{\Delta n}{n}| \gg |\frac{\Delta\tau}{\tau}|$ with temperature rise, the $\frac{\Delta\sigma}{\sigma}$ is expected to be positively large. The similar changes in the experimental ρ is seen from ~ 2.5 to 200 K as mentioned earlier²⁶⁻²⁹. Thus, from Fig. 4(a) for 612 Bohr³ the presence of sharp edges around the E_F appear to be responsible for making $|\frac{\Delta n}{n}| \gg |\frac{\Delta\tau}{\tau}|$ with per Kelvin rise in temperature around 100 K. Now on looking at the Fig. 4(b) for 612 Bohr³, shallowing of DOS near to E_F is observed which will reduce the value of $\frac{\Delta n}{n}$ with per Kelvin rise in temperature around 300 K, resulting in lowering the difference between $\frac{\Delta n}{n}$ and $\frac{\Delta\tau}{\tau}$ with increase in temperature. As a result, it is now expected to follow the relation, where $|\frac{\Delta n}{n}| > |\frac{\Delta\tau}{\tau}|$ and this will make $\frac{\Delta\sigma}{\sigma}$ to decrease around 300 K which is also observed in the experimental data²⁶⁻²⁹, suggesting the material to be less insulating than 100 K. Hence, the profiling of the temperature-dependent DOS around the Fermi level is playing an important role in deciding the transport behavior of the material. Then, on looking at Fig. 4(b)-4(c) for the 300-800 K, we have observed reverse effects over the DOS near to E_F . The sharp edges are again forming, refining the line shape of DOS around E_F with an emergence of peak 2 unlike 300 K result. Peak 1 has moved closer to the E_F while peaks corresponding to 551

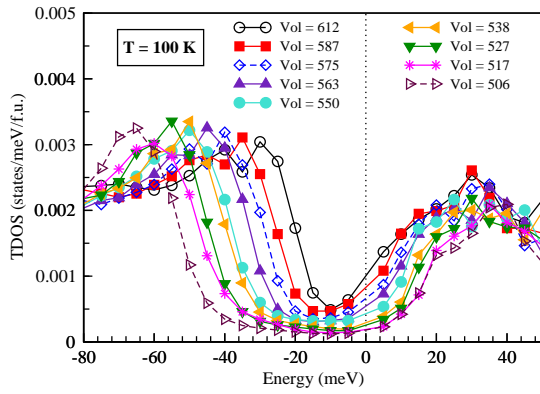


FIG. 5. (color online) TDOS calculated within DFT+DMFT for FeSi at 100 K for different unit cell volumes ranging from 612 to 507 Bohr³. Zero energy corresponds to the Fermi level.

and 507 Bohr³ volumes have moved away. The formation of sharp edge is such that DOS near E_F got increased in a very minimal amount for 612 Bohr³ in comparison to its 100 K result. Here again, sharp edge of DOS suggesting that there is a possibility of larger $\frac{\Delta n}{n}$ with per Kelvin rise in temperature. This relative change of n is expected to be reflected in transport behavior of the material with its insulating state. As no experiments have been found for 800 K, there's a possibility of witnessing this unusual behavior when one performs any transport measurement at high temperature for 612 Bohr³ volume.

Now, looking again at Fig. 4(a) to 4(c), we have found few changes with decrease in volume *viz.* (i) the DOS near to E_F are diminishing at each temperature and (ii) changes in the energy positions of peaks 2 and 3 corresponding to 551 and 507 Bohr³. For instance, for 100 K at ~ -5 meV the DOS is ~ 0.0006 states/meV/f.u. for the 612 Bohr³, which has reached upto ~ 0.0001 states/meV/f.u. for the 507 Bohr³. Starting from 100 K, we have seen sharp edges for 612 Bohr³ which signified sharp decrement in ρ (discussed above), showing the existence of an insulating state there. So, with decreasing volume the deep well has gone down further with lesser DOS than 612 Bohr³, and thus insulating behavior is expected to be followed for the rest volumes leading to the formation of energy gap for 100 K. Then at 300 K in Fig. 4(b), we have seen shallower DOS around E_F indicating the material to be less insulating for 612 Bohr³ in accordance with experimental ρ observation. But now for 300 K, with volume decrement sharp edges have again formed with almost negligible DOS. As we already know sharp edges are direct replica for greater change in $\frac{\Delta n}{n}$ with per Kelvin rise in temperature. Thus, for the rest reduced volumes i.e., 551 and 507 Bohr³ around 300 K, the material is expected to be in its semi-conducting state. Based on this, it seems like with decreasing volume semiconductor to metal transition temperature to shift towards higher temperature. Besides, it is already known that non-magnetic feature is associated with semi-conducting

state of materials. Thus, it seems like with decreasing volume non-magnetic to magnetic transition can be expected to be observed here for this material. Now moving onto 800 K in Fig. 4(c), we found that the decreasing trend of DOS near E_F is still followed here. Thus, here again a similar behavior of the material is expected to follow as it happened in 100 K w.r.t reduced volumes. Hence, it can be said that for FeSi with decreasing volumes at any absolute temperature, its conductivity will decrease which is unlike other materials where on application of pressure their conductivity increases⁸¹⁻⁸³. Furthermore for the representation purpose, we have shown the plot for TDOS at 100 K for all the unit cell volumes in the range 612 to 507 Bohr³ in the Fig. 5. Suggesting the possibility of getting a clean gap for the material with further reduction of the unit cell volume.

In continuation with density of states and to realize the results obtained, we have plotted DMFT obtained momentum-resolved spectral function along various high symmetry lines at extreme temperature $T = 800$ K for three volumes (a) 612 Bohr³ (b) 551 Bohr³ and (c) 507 Bohr³ in Fig. 6(a) - 6(c). Generally, it is said that DOS are exact replica of Brillouin zone while band structure shows one part of Brillouin zone in some well defined high symmetric k -points. However, the obtained spectral function is able to reflect the obtained results as discussed in our DOS section. Likewise, when we move from Fig. 6(a)- 6(c), two major changes are observed with volume compression *viz.* (i) the metal-insulator transition is clearly evident here and (ii) the decrease in the incoherency of the spectrum i.e., more sharp dispersions indicating increment in coherent weight. Here, it is important to note that while observing dispersions within DFT, one can find electron has one discrete energy ($\epsilon_0(k)$) for the given k -point and n^{th} band. The spectral function $A(k, \omega)$ has a δ -function peak at $\omega = \epsilon_0(k)$, and n & k are good quantum numbers. However, within DMFT now the same electron has a range of energies at the same given k -point & n^{th} band, and n & k are no longer good quantum numbers. So, on plotting $A(k, \omega)$ for the same given k -point and n^{th} band, the plot will look like the figure given in Fig.1(b) in⁸⁴ where there will be one sharp peak (with broadening in shape) and rest of the spectrum contains broadened structures. The sharp peak shown in the figure will correspond to DFT obtained δ peak which has now broadened and normally it is expected to be shifted from its energy position; this peak is associated with coherent weight. On other side, all other broadened structures seen in the figure other than the sharp one is then associated with incoherent weight. But, when we go for larger numbers of n and k -points, the overall spectrum will have smeared features along with sharp dispersive lines. Here, the smearing of spectrum is associated with incoherent weight (states with shorter lifetime) while the sharp dispersions with coherent weight (states with longer lifetime). Thus, observing Fig. 6(a) for 612 Bohr³, we found smeared features nearer to the Fermi level around $-0.05 \text{ eV} \leq \omega \leq 0.05 \text{ eV}$ in the direction of

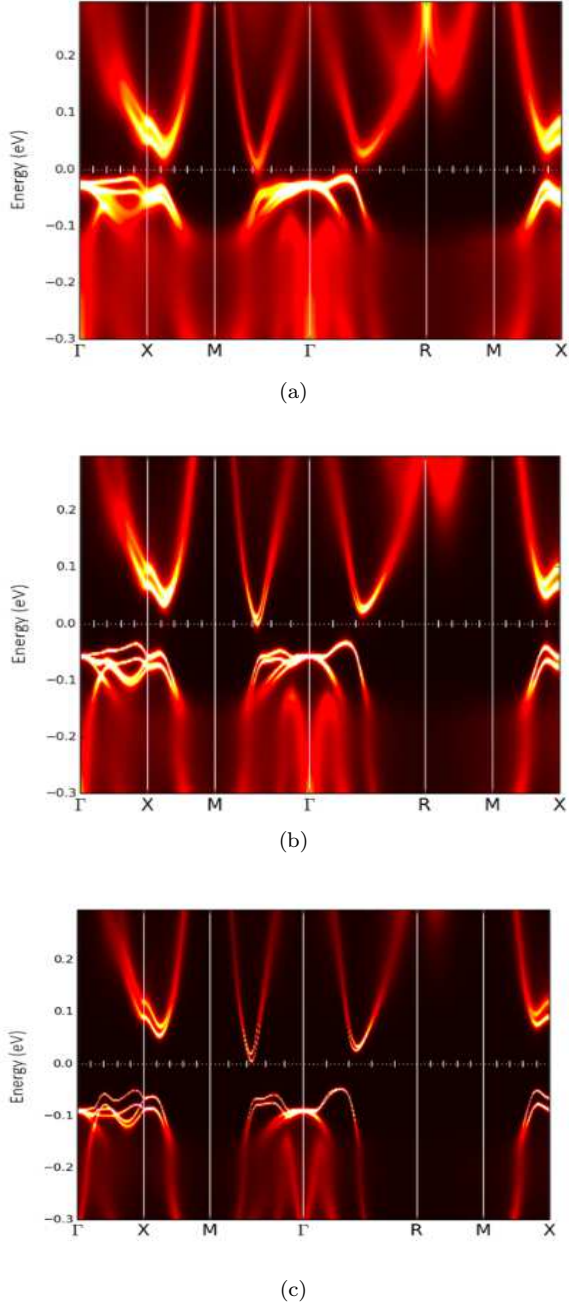


FIG. 6. (colour online) Momentum-resolved many-body spectral function at $T = 800$ K for volumes (a) $V = 612 \text{ Bohr}^3$, (b) $V = 551 \text{ Bohr}^3$, and (c) $V = 507 \text{ Bohr}^3$ for FeSi. Zero energy is the Fermi level.

Γ -M- Γ and M-X. This indicates the presence of incoherent states in that energy window, and also making the material to exhibit its metallic state. But, on moving to Fig. 6(b) and 6(c), the smearing of features are reducing on volume reduction, indicating increment in coherent weight i.e., incoherency of the spectrum has decreased. In consequence of which very less incoherent states (almost negligible) are seen around the Fermi level giving a clean semi-conducting gap when looked at Fig. 6(c).

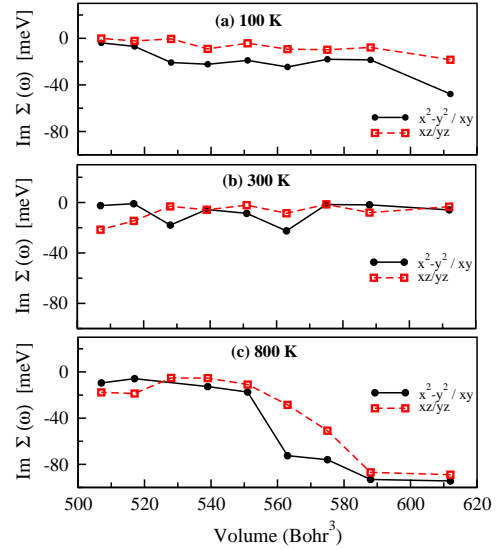


FIG. 7. (color online) Imaginary parts of the self-energy ($\text{Im } \Sigma(\omega)$) for orbital components x^2-y^2/xy and xz/yz of Fe $3d$ states nearer to the Fermi level as a function of volume for (a) 100 K, (b) 300 K and (c) 800 K.

This kind of result is predicted from DOS in Fig. 4(a) - 4(c). Interestingly, in our previous work⁴⁵ and Tomczak *et al.* work, we have seen that with rise in temperature the spectrum is supposed to be incoherent while here in this Fig. 6(a) - 6(c), we found that in spite of high temperature $T=800$ K, the incoherency has got reduced with volume reduction.

Next, we have shown the plot of imaginary parts of self-energy ($\text{Im } \Sigma(\omega)$) for orbital components x^2-y^2/xy and xz/yz of Fe $3d$ states nearer to the Fermi level as a function of volume for (a) 100 K, (b) 300 K and (c) 800 K in Fig. 7(a) - 7(c). $\text{Im } \Sigma(\omega)$ values for x^2-y^2/xy and xz/yz orbital components are calculated for $\omega \sim -0.11$ eV and ~ 0.23 eV, respectively. Here, it is important to note that only these orbitals are chosen on the basis of our last work⁴⁵, where we found that these orbitals x^2-y^2/xy and xz/yz are contributing most, one in the VB and other in CB, respectively. $\text{Im } \Sigma(\omega)$ provides the information regarding lifetime of quasiparticle states. More is the value of $\text{Im } \Sigma(\omega)$ more will be the lifetime broadening and more will be the quasiparticle-

TABLE III. Calculated m^* for the reduced unit cell volumes at $T = 800$ K

Orbital component	Unit cell volume		
	612 (Bohr ³)	551 (Bohr ³)	507 (Bohr ³)
x^2-y^2/xy	1.83	1.52	1.42
xz/yz	1.73	1.52	1.42

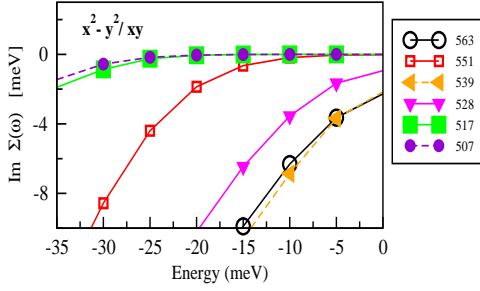


FIG. 8. (color online) Imaginary parts of self-energy ($\text{Im}\Sigma(\omega)$) for orbital components x^2-y^2/xy of Fe 3d states nearer to the Fermi level in the occupied region with respect to different reduced volumes for 300 K.

quasiparticle scatterings. So, when we look at the Fig. 7(a)-7(c) for 612 Bohr³ volume, we found that with rise in temperature the value of $\text{Im}\Sigma(\omega)$ for x^2-y^2/xy orbital component has first gone down (magnitude wise) from ~ -47 meV to -5 meV for 100-300 K and then reaches upto ~ -94 meV at 800 K. This indicates that the lifetime of quasiparticles to be very large around 300 K i.e., more coherent weight and then the lifetime decreases when it reaches 800 K. Normally, it is said that larger value of lifetime of quasiparticles leads to lesser possibility of quasiparticles-quasiparticles scatterings which means the relaxation time (τ) to be large. Accordingly, for 612 Bohr³ volume with rise in temperature the τ value seems to be large at ~ 300 K while it might decrease from 300-800 K. Now, on observing for other volumes at 100, 300 and 800 K, we found that with volume compression, the value of $\text{Im}\Sigma(\omega)$ is decreasing indicating enhancement of lifetime broadening for both the orbitals. Here again, the value of $\text{Im}\Sigma(\omega)$ is extremely small at 300 K if compared with 100 K and 800 K plot in Fig. 7(a) to 7(c). Thus, more coherent states to exist around this temperature for all the reduced volumes with lesser possibility of quasiparticles-quasiparticles scatterings. This observation of increased coherency of spectrum is also going with Table III data, where we have calculated the effective band mass-renormalization parameter (m^*) at $T = 800$ K for three distinct volumes $\sim 612, 551$ & 507 Bohr³. The m^* is calculated from the relation $m^* = 1 - (d\text{Re}\Sigma(\omega)/d\omega)|_{\omega=0}$, and m^* is arising from many-body effects. From Table III, we observed that with volume reduction, the value of m^* is also decreasing indicating transfer of spectral weights from incoherent states to coherent states, and making spectrum less & less incoherent. The existence of more coherent states is also evident from Fig. 6(a) to 6(c), where incoherency in spectrum has reduced.

For the further continuation, we have shown another plot of $\text{Im}\Sigma(\omega)$ as contributed by orbital components x^2-y^2/xy of Fe 3d states nearer to the Fermi level in the occupied region with respect to different reduced volumes for 300 K in Fig. 8. Here again, we have observed a sim-

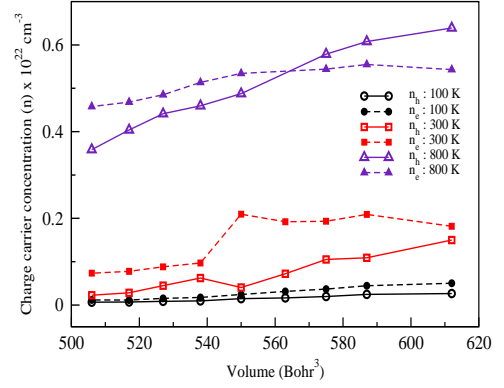


FIG. 9. (color online) Variations in number of charge carriers around the Fermi level (E_F) with volume compression within energy range from ~ -9 meV to 9 meV, ~ -25 meV to 25 meV and ~ -70 meV to 70 meV corresponding to temperatures 100 K, 300 K and 800 K, respectively.

ilar trend exhibited by the quasiparticle states which are becoming more and more coherent with volume decrement. Likewise, if one follows the slopes of the curves we found that they are decreasing from ~ -0.6 to ~ 0.08 for volumes 563 Bohr³ to 507 Bohr³, respectively. It is directly showing that the lifetime of quasiparticles are becoming larger and larger which is almost infinite. Hence, we can say that here LFL theory seems to be followed within the range of volumes 612 to 507 Bohr³ for this material. This is also in accordance with Tomczak *et al.* result⁴⁴ where LFL is followed for 612 bohr³ volume of FeSi.

Next, we have studied the changes occurring in the number of charge carriers (around the E_F) mainly participating in conduction with the reduction of unit cell volumes. Accordingly, we have plotted variations found in charge carrier concentration within the $k_B T$ range for all the three different temperatures. Likewise, for 100 K, 300 K and 800 K, the range is for ~ -9 meV to 9 meV, ~ -25 meV to 25 meV and ~ -70 meV to 70 meV, respectively, in the Fig. 9. For plotting this figure, we have calculated the number of electrons (n_e) and holes (n_h) lying within the set range by evaluating the areas under the curve by method of integration. From the plot for the temperatures 100-300 K, we observed that for the Vol = 612 Bohr³ $n_e > n_h$ which is followed by all the volumes. This outcome is according to the negative Hall coefficient as observed experimentally^{2,32}. This Fig. 9 has shown the same decrement in the charge carriers with volume reduction as seen above. This further shows the decrement in the conductivity of the material with the volume decrement. However, when we move from 300 K to 800 K, a reverse effect is observed here i.e., $n_e < n_h$ until vol = 575 Bohr³ while after this volume n_e becomes greater than n_h . This kind of unusual behavior of FeSi might be attributed with the large particle-hole asymmetry with volume decrement seen in TDOS at 800

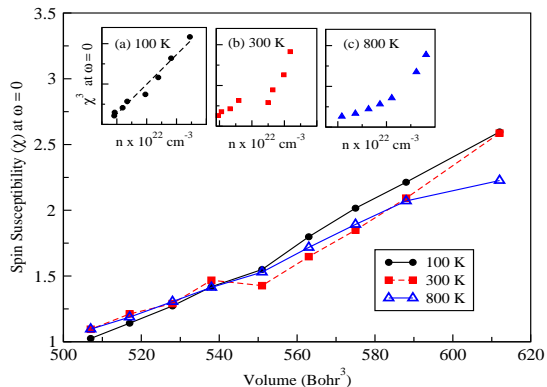


FIG. 10. (color online) Spin susceptibility (χ) at $\omega = 0$ (calculated within DFT+DMFT) versus unit cell volumes ranging from 612 to 507 Bohr³ for 100 K, 300 K and 800 K, respectively.

K from Fig. 4(c). It will be quite interesting if one performs the Hall experiment at high temperature for this material to witness its unusual effect of reduced volumes.

In this part of results and discussion, we have presented the plot for the calculated spin susceptibility (χ) at $\omega = 0$ versus unit cell volumes ranging from 612 to 507 Bohr³ for three distinct temperatures in Fig. 10. This χ is basically providing the information of the spin-spin correlations. From the plot we have found that χ for 612 Bohr³ volume has a value of ~ 2.6 at both 100 K and 300 K whereas the value got reduced to ~ 2.2 for 800 K. The figure shows a decreasing trend of χ value with reducing unit cell volumes. At this moment, if one follows the experimental magnetic susceptibility measurement as performed by Petrova *et al.*²⁶, one can see that with lower temperatures below 100 K, FeSi is in non-magnetic state with almost negligible value of magnetic susceptibility while above 100 K its value keeps increasing till 300 K. From their plot, it seems to observe a transition temperature around 100 K from its non-magnetic state to magnetic state. Now, observing the decreasing value of χ with volume reduction in the Fig. 10, it seems like with volume decrement the transition temperature may also be shifting towards lower temperatures. Moreover, we have observed that the nature of decrement in χ with volume reduction is similar to the decrement in charge carrier concentration (n). For Pauli paramagnetic materials, it is already known that their susceptibility is directly proportional to the DOS at E_F , and given by the equation $\chi = \mu_B^2 g(\epsilon_F)$, where $g(\epsilon_F)$ is the DOS at E_F ⁸⁰. At the same time from free-electron theory, $g(\epsilon_F) = \frac{m}{\hbar^2 \pi^2} (3\pi^2 n)^{1/3}$, and consequently, one can write $\frac{\chi^3}{n} = \text{constant}$. This shows that if any material follows this linearity relation then it seems to be Pauli paramagnetic in nature. So moving in this direction, we have drawn insets inside this figure where a plot of χ^3 versus n for (a) 100 K, (b) 300 K and (c) 800 K are given. For the 100 K case, a linear fit has also been done and found

to be almost fitted with the data points as seen in Fig 10(a). Thus, we have observed that at 100 K FeSi appears to follow the linearity relation. However, for both 300 K and 800 K in Fig. 10(b)-10(c), we have found that their nature of plot has deviated from the linear behavior. Plots of 300 K and 800 K seem to follow $\frac{\chi^3}{n^2} = \text{constant}$ relation. Hence from the Fig 10(a)-10(c), it appears that FeSi is Pauli paramagnetic around 100 K for all reduced volumes, whereas it is not the case around 300 K and above.

In the end of the results and discussions, we would like to add further observations regarding the probable electronic configurations of Fe 3d orbitals. Mixed configurations with d^5-d^8 (most probable as d^7) are found again, and these configurations are found to be pressure and temperature independent. This result is similar to our earlier work⁴⁵, indicating that reduction in volume does not have any further effect over its electronic configuration.

IV. CONCLUSION

In this work, we have shown how the pressure and temperature can play an important role in understanding the underlying rich physics for the electrical and magnetic properties of FeSi. This study is mainly aimed at resolving the unusual magnetic susceptibility behavior of FeSi around 100-300 K by carrying out DFT+DMFT calculations. At first, we started with calculating the a_0 and B_0 values (~ 4.32 Å and 110 GPa, respectively,) from the free energy as evaluated within DMFT method at 300 K. These calculated values are found to be quite close to the experimental results. From DFT calculations, the increment in bandgap of the material with volume decrement is observed, and unit cell volume of ~ 769 Bohr³ is found to have zero bandgap.

From DMFT calculations a profound effect of U and temperature is found, and due to which at ~ 300 K the bandgap got filled up with incoherent states. However, with the application of pressure the number of states per unit volume (n) available around the Fermi level got reduced with volume decrement from 612 to 507 Bohr³; indicating reduction in its electrical conductivity. As a result metal-insulator transition (MIT) is witnessed at ~ 300 K with volume compression. Profiling of temperature-dependent DOS is quite appropriately explaining the behavior of experimental electrical resistivity data. Here, coherency of spectrum has increased with volume compression even at higher temperatures. Around 300-800 K, $n_e < n_h$ until vol = 575 Bohr³ while after this volume n_e becomes greater than n_h is found. This will be quite interesting for the experimentalists, if they happen to perform the Hall experiment at high temperature to witness this unusual effect of volume compression. Moreover, a similar decreasing trend in χ is observed as in n with volume reduction and following $\frac{\chi^3}{n} = \text{constant}$ relation for ~ 100 K, showing FeSi to be

Pauli paramagnetic at ~ 100 K. The present work clearly shows the applicability of controllable parameters such as pressure and temperature for exploring this class of $3d$ transition metal monosilicides with the help of advance

formulation as employed in DFT+DMFT technique.

V. REFERENCES

-
- * dutta.paromita1@gmail.com
† sudhir@iitmandi.ac.in.com
- ¹ G. Kotliar and D. Vollhardt, *Physics Today* **3**, 53 (2004).
 - ² M. Imada, A. Fujimori, and Y. Tokura, *Rev. Mod. Phys.* **70**, 1039 (1998).
 - ³ E. Morosan, D. Natelson, A. H. Nevidomskyy, and Q. Si, *Adv. Mater.* **24**, 4896 (2012).
 - ⁴ J. Beille, J. Voiron, and M. Roth, *Solid State Commun.* **47**, 399 (1983).
 - ⁵ M. A. Chernikov, L. Degiorgi, E. Felder, S. Paschen, A. D. Bianchi, H. R. Ott, J. L. Sarrao, Z. Fisk, and D. Mandrus, *Phys. Rev. B* **56**, 1366 (1997).
 - ⁶ J. Beille, J. Voiron, F. Towfiq, M. Roth, and Z. Y. Zhang, *J. Phys. F: Met. Phys.* **11**, 2153 (1981).
 - ⁷ N. Manyala, Y. Sidis, J. F. DiTusa, G. Aeppli, D. P. Young, and Z. Fisk, *Nature (London)* **404**, 581 (2000).
 - ⁸ N. Manyala, Y. Sidis, J. F. DiTusa, G. Aeppli, D. P. Young, and Z. Fisk, *Nat. Mater.* **3**, 255 (2004).
 - ⁹ S. Yeo, S. Nakatsuji, A. D. Bianchi, P. Schlottmann, Z. Fisk, L. Balicas, P. A. Stampe, and R. J. Kennedy, *Phys. Rev. Lett.* **91**, 046401 (2003).
 - ¹⁰ V. I. Anisimov, R. Hlubina, M. A. Korotin, V. V. Mazurenko, T. M. Rice, A. O. Shorikov, and M. Sigrist, *Phys. Rev. Lett.* **89**, 257203 (2002).
 - ¹¹ T. Jarlborg, *J. Magn. Magn. Mater.* **283**, 238 (2004).
 - ¹² P. Pedrazzini, H. Wilhelm, D. Jaccard, T. Jarlborg, M. Schmidt, M. Hanfland, L. Akselrud, H. Q. Yuan, U. Schwarz, Y. Grin, and F. Steglich, *Phys. Rev. Lett.* **98**, 047204 (2007).
 - ¹³ S. Patankar, S. K. Pandey, V. R. Reddy, A. Gupta, A. Banerjee, and P. Chaddah, *Europhys. Lett.* **90**, 57007 (2010).
 - ¹⁴ S. Lal and S. K. Pandey, *Mater. Res. Express* **3**, 116301 (2016).
 - ¹⁵ S. Lal and S. K. Pandey, *Comput. Mater. Sci.* **126**, 373 (2017).
 - ¹⁶ S. K. Pandey, *Phys. Rev. B* **86**, 085103 (2012).
 - ¹⁷ C. Pfleiderer, P. Böni, T. Keller, U. K. Rößler, and A. Rosch, *Science* **316**, 1871 (2007).
 - ¹⁸ T. Schulz, R. Ritz, A. Bauer, M. Halder, M. Wagner, C. Franz, C. Pfleiderer, K. Everschor, M. Garst, and A. Rosch, *Nat. Phys.* **8**, 301 (2012).
 - ¹⁹ G. Föex, *J. Phys. Radium* **9**, 37 (1938).
 - ²⁰ V. Jaccarino, G. K. Wertheim, J. H. Wernick, L. R. Walker, and S. Araj, *Phys. Rev.* **160**, 476 (1967).
 - ²¹ G. K. Wertheim, V. Jaccarino, J. H. Wernick, J. A. Seitchik, H. J. Williams, and R. C. Sherwood, *Phys. Lett.* **18**, 89 (1965).
 - ²² H. Watanabe, H. Yamamoto, and K.-i. Ito, *J. Phys. Soc. Jpn.* **18**, 995 (1963).
 - ²³ Y. Takahashi, M. Tano, and T. Moriya, *J. Magn. Magn. Mater.* **31-34**, 329 (1983).
 - ²⁴ Y. Takahashi and T. Moriya, *J. Phys. Soc. Jpn.* **46**, 1451 (1979).
 - ²⁵ S. N. Evangelou and D. M. Edwards, *J. Phys. C* **16**, 2121 (1983).
 - ²⁶ A. E. Petrova, V. N. Krasnorussky, A. A. Shikov, W. M. Yuhasz, T. A. Lograsso, J. C. Lashley, and S. M. Stishov, *Phys. Rev. B* **82**, 155124 (2010).
 - ²⁷ A. Sakai, S. Yotsuhashi, H. Adachi, F. Ishii, Y. Onose, Y. Tomioka, N. Nagaosa, and Y. Tokura, in *26th International Conference on Thermoelectrics* (2007) p. 256.
 - ²⁸ T. Ou-Yang, Y. Zhuang, B. Ramachandran, W. Chen, G. Shu, C. Hu, F. Chou, and Y. Kuo, *J. Alloys Compd.* **702**, 92 (2017).
 - ²⁹ T. Y. Ou-Yang, G. J. Shu, and H. R. Fuh, *Europhys. Lett.* **120**, 17002 (2017).
 - ³⁰ R. Wolfe, J. H. Wernick, and S. E. Haszko, *Phys. Lett.* **19**, 449 (1965).
 - ³¹ M. Fäth, J. Aarts, A. A. Menovsky, G. J. Nieuwenhuys, and J. A. Mydosh, *Phys. Rev. B* **58**, 15483 (1998).
 - ³² V. I. Kaidanov, V. A. Tselishchev, I. K. Iesalniek, L. D. Dudkin, B. K. Voronov, and N. N. Trusova, *Sov. Phys. Semicond.* **2**, 382 (1968).
 - ³³ G. Shirane, J. E. Fischer, Y. Endoh, and K. Tajima, *Phys. Rev. Lett.* **59**, 351 (1987).
 - ³⁴ S.-J. Oh, J. W. Allen, and J. M. Lawrence, *Phys. Rev. B* **35**, 2267 (1987).
 - ³⁵ L. F. Mattheiss and D. R. Hamann, *Phys. Rev. B* **47**, 13114 (1993).
 - ³⁶ Z. Fisk, J. L. Sarrao, S. L. Cooper, P. Nyhus, G. S. Boebinger, A. Passner, and P. C. Canfield, *Physica B: Condensed Matter* **223-224**, 409 (1996).
 - ³⁷ T. E. Mason, G. Aeppli, A. P. Ramirez, K. N. Clausen, C. Broholm, N. Stücheli, E. Bucher, and T. T. M. Palstra, *Phys. Rev. Lett.* **69**, 490 (1992).
 - ³⁸ K. Urasaki and T. Saso, *J. Phys. Soc. Jpn* **68**, 3477 (1999).
 - ³⁹ K. Urasaki and T. Saso, *Phys. Rev. B* **58**, 15528 (1998).
 - ⁴⁰ C. M. Varma, *Phys. Rev. B* **50**, 9952 (1994).
 - ⁴¹ J. Kuneš and V. I. Anisimov, *Phys. Rev. B* **78**, 033109 (2008).
 - ⁴² C. Fu and S. Doniach, *Phys. Rev. B* **51**, 17439 (1995).
 - ⁴³ V. V. Mazurenko, A. O. Shorikov, A. V. Lukoyanov, K. Kharlov, E. Gorelov, A. I. Lichtenstein, and V. I. Anisimov, *Phys. Rev. B* **81**, 125131 (2010).
 - ⁴⁴ J. M. Tomczak, K. Haule, and G. Kotliar, *Proc. Natl Acad. Sci.* **109**, 3243 (2012).
 - ⁴⁵ P. Dutta and S. K. Pandey, *J. Phys. Condens. Matter* **31**, 145602 (2019).
 - ⁴⁶ Y. Yanagi and K. Ueda, *Phys. Rev. B* **93**, 045125 (2016).
 - ⁴⁷ Z. Schlesinger, Z. Fisk, H.-T. Zhang, M. B. Maple, J. DiTusa, and G. Aeppli, *Phys. Rev. Lett.* **71**, 1748 (1993).
 - ⁴⁸ A. Lacerda, H. Zhang, P. Canfield, M. Hundley, Z. Fisk, J. Thompson, C. Seaman, M. Maple, and G. Aeppli, *Physica B: Condensed Matter* **186-188**, 1043 (1993).
 - ⁴⁹ B. C. Sales, E. C. Jones, B. C. Chakoumakos, J. A. Fernandez-Baca, H. E. Harmon, J. W. Sharp, and E. H.

- Volckmann, Phys. Rev. B **50**, 8207 (1994).
- ⁵⁰ M. Mihalik, M. Timko, P. Samuely, N. Tomaoviova-Hudkova, P. Szab, and A. Menovsky, J. Magn. Magn. Mater. **157-158**, 637 (1996).
- ⁵¹ P. Samuely, P. Szabó, M. Mihalik, N. Hudáková, and A. A. Menovsky, Physica B Condensed Matter **218**, 185 (1996).
- ⁵² L. Degiorgi, M. B. Hunt, H. R. Ott, M. Dressel, B. J. Feenstra, G. Grner, Z. Fisk, and P. Canfield, Europhys. Lett. **28**, 341 (1994).
- ⁵³ O. Delaire, K. Marty, M. B. Stone, P. R. C. Kent, M. S. Lucas, D. L. Abernathy, D. Mandrus, and B. C. Sales, Proc. Natl Acad Sci. **108**, 4725 (2011).
- ⁵⁴ C. Fu, M. P. C. M. Krijn, and S. Doniach, Phys. Rev. B **49**, 2219 (1994).
- ⁵⁵ V. R. Galakhov, E. Z. Kurmaev, V. M. Cherkashenko, Y. M. Yarmoshenko, S. N. Shamin, A. V. Postnikov, S. Uhlenbrock, M. Neumann, Z. W. Lu, B. M. Klein, and Z.-P. Shi, J. Phys.: Condens. Matter **7**, 5529 (1995).
- ⁵⁶ G. Grechnev, T. Jarlborg, A. Panfilov, M. Peter, and I. Svehkarev, Solid State Commun. **91**, 835 (1994).
- ⁵⁷ V. I. Anisimov, S. Y. Ezhov, I. S. Elfimov, I. V. Solovyev, and T. M. Rice, Phys. Rev. Lett. **76**, 1735 (1996).
- ⁵⁸ T. Jarlborg, Phys. Rev. B **51**, 11106 (1995).
- ⁵⁹ M. Arita, K. Shimada, Y. Takeda, M. Nakatake, H. Namatame, M. Taniguchi, H. Negishi, T. Oguchi, T. Saitoh, A. Fujimori, and T. Kanomata, Phys. Rev. B **77**, 205117 (2008).
- ⁶⁰ K. Haule, C.-H. Yee, and K. Kim, Phys. Rev. B **81**, 195107 (2010).
- ⁶¹ K. Haule and T. Birol, Phys. Rev. Lett. **115**, 256402 (2015).
- ⁶² V. I. Anisimov and O. Gunnarsson, Phys. Rev. B **43**, 7570 (1991).
- ⁶³ G. K. H. Madsen and P. Novák, Europhys. Lett. **69**, 777 (2005), cond-mat/0412560.
- ⁶⁴ P. Blaha, K. Schwarz, G. K. H. Madsen, D. Kvasnicka, and J. Luitz, An augmented plane wave + local orbitals program for calculating crystal properties (2001).
- ⁶⁵ B. Bofen and A. Kemi, Min. Geol. **11A**, 1 (1933).
- ⁶⁶ R. O. Jones and O. Gunnarsson, Rev. Mod. Phys. **61**, 689 (1989).
- ⁶⁷ F. Birch, Phys. Rev. **71**, 809 (1947).
- ⁶⁸ P. Dutta and S. K. Pandey, Comput. Condens. Matter **16**, e00325 (2018).
- ⁶⁹ S. Lal and S. K. Pandey, Phys. Lett. A **381**, 2117 (2017).
- ⁷⁰ P. Dutta, S. Lal, and S. K. Pandey, Eur. Phys. J. B **91**, 183 (2018).
- ⁷¹ P. Dutta, S. Lal, and S. K. Pandey, AIP Conf. Proc. **1942**, 090017 (2018).
- ⁷² K. Haule, Phys. Rev. B **75**, 155113 (2007).
- ⁷³ K. Haule, Phys. Rev. Lett. **115**, 196403 (2015).
- ⁷⁴ M. Jarrell and J. E. Gubernatis, Phys. Rep. **269**, 133 (1996).
- ⁷⁵ E. Knittle and Q. Williams, Geophys. Res. Lett. **22**, 445 (1995).
- ⁷⁶ J. F. Lin, A. Campbell, D. L. Heinz, and G. Shen, J. Geophys. Res. **108(B1)**, 2045 (2003a).
- ⁷⁷ I. G. Wood, W. I. F. David, S. Hull, and G. D. Price, J. Appl. Crystallogr. **29**, 215 (1996).
- ⁷⁸ F. Guyot, J. Zhang, I. Martinez, J. Matas, Y. Ricard, and M. Javoy, Eur. J. Mineral. **9**, 277 (1997).
- ⁷⁹ G. P. Zinoveva, L. P. Andreeva, and P. V. Geld, Phys. Status Solidi A **23**, 711 (1974).
- ⁸⁰ N. Ashcroft and N. Mermin, *Solid State Physics* (Cengage Learning, 2011).
- ⁸¹ N. F. Mott, Proceedings of the Physical Society. Section A **62**, 416 (1948).
- ⁸² D. B. McWhan, A. Menth, J. P. Remeika, F. Brinkman, and T. M. Rice, Phys. Rev. B **7**, 1920 (1973).
- ⁸³ S. A. Carter, T. F. Rosenbaum, M. Lu, H. M. Jaeger, P. Metcalf, J. M. Honig, and J. Spalek, Phys. Rev. B **49**, 7898 (1994).
- ⁸⁴ G. Kotliar, S. Y. Savrasov, K. Haule, V. S. Oudovenko, O. Parcollet, and C. A. Marianetti, Rev. Mod. Phys. **78**, 865 (2006).